ISSN-1996-918X

Pak. J. Anal. Environ. Chem. Vol. 26, No. 2 (2025) 299 – 309

http://doi.org/10.21743/pjaec/2025.12.10

Morphology and Filtration Characteristics of a Polysulfone Hollow Fiber Membrane

Sultan K. Alharbi[1], Muhammad M. Shaikh[1], Abdullah I. AlZarah[2], SalahEldin A. ElAmin[2], Saleh O. AlAswad[2] and Awadh O. AlSuhaim[1]*

[1]*Chemistry Department, Faculty of Sciences, Taibah University, P.O. Box 30002, Al Medina Al Munawarah, Saudi Arabia.*

[2]*National Center for Water Treatment and Desalination Technology, P.O. Box 6086 Riyadh 11442, Saudi Arabia.*

*Corresponding author Email: mansoorishaque@gmail.com

Received 21 August 2025, Revised 29 October 2025, Accepted 05 November 2025

Academic Editor: Huma Mudassar

Abstract

Polysulfone (PSF) hollow fiber membranes incorporating a asymmetric microstructures suitable for ultrafiltration, were fabricated using dry–wet phase inversion method. The optimized dope solution contained PSF (25 wt%), polyethylene glycol (PEG-400; 22 wt%), and polyvinylpyrrolidone (PVP-K90, Mw ≈ 1,300 kDa; 0.3 wt%) dissolved in N,N-dimethylacetamide (52.7 wt%). The extruded nascent fibers coagulated in deionized water to form membranes with a dense selective skin layer supported by a porous substructure. Fourier Transform Infrared Spectroscopy (FT-IR) analysis confirmed the presence of the characteristic sulfone functional groups, indicating the chemical stability of the PSF matrix. Scanning Electron Microscopy (SEM) revealed a well-defined lumen structure with a diameter of 1.09 ± 0.05 mm and a wall thickness of 0.20 ± 0.01 mm. The membrane cross-section showed distinct finger-like macrovoids. These extended throughout the structure, indicating effective phase inversion and stable morphology. The membrane exhibited a porosity of 48.8 ± 2.1% and a pure water permeance of 70 ± 5 L m^{-2} h^{-1} bar^{-1}. The evaluation of ultrafiltration performance was done using bovine serum albumin (BSA, Mw ≈ 66 kDa). The membrane showed a rejection rate of 95 ± 1% at 2 bar pressure. This confirms its effective size-exclusion capability. Compared with reported PSF flat-sheet membranes, the present hollow fiber configuration demonstrated a more favourable balance between permeability and selectivity, attributed to PEG-400-driven rapid demixing and PVP-induced pore interconnectivity. These findings showcase the potential of this minimalist dual-additive formulation for scalable, high-performance PSF hollow fiber membranes in aqueous separation applications.

Keywords: polysulfone hollow fiber membrane, PEG-400, PVP, phase inversion, morphology, ultrafiltration.

Introduction

Low-pressure membrane processes, including microfiltration (MF) and ultrafiltration (UF), are widely employed in water and wastewater treatment systems for the removal of particulates, colloids, and natural organic matter (NOM) [1]. Among the various polymers used for UF membrane fabrication, polysulfone (PSF) is one of the most prominent due to its excellent thermal stability, mechanical strength, and chemical resistance [2-4]. The successful fabrication of PSF hollow fiber membranes

depends on the careful optimization of numerous parameters, including spinning conditions, air gap distance, take-up speed, shear rate, polymer concentration, dope viscosity, bore liquid composition, and additive selection [5]. Each factor influences the phase inversion kinetics, thereby determining the membrane morphology and performance. The composition of polymer dope solution and the nature of the additives play a decisive role in the formation of membrane microstructure. High-performance UF membranes typically exhibit a thin selective skin layer, minimal macrovoids, and a well-developed porous substructure [6]. The dry–wet phase inversion method is the most common approach for fabricating asymmetric PSF membranes, as it allows fine control over pore architecture and layer thickness [7-9]. Although high permeability is essential for efficient separation, it often compromises membrane selectivity. To address this trade-off, polyethylene glycol (PEG) is commonly employed as a pore-forming agent. Its addition promotes phase separation and increases hydrophilicity, which could enhance water permeability. However, excessive PEG loading can enlarge pore size, leading to reduced solute rejection [10–12].

The effect of PEG molecular weight on membrane morphology is well-established. PEGs with molecular weights ranging from 400 to 20,000 Da generally increase pore size and porosity, resulting in improved flux performance [13]. Among these, PEG-400 has demonstrated particular effectiveness at concentrations up to 10 wt%, where it facilitates solvent–nonsolvent exchange and reduces surface resistance, ultimately optimizing porosity and filtration efficiency [14,15].

In parallel, polyvinylpyrrolidone (PVP) is another widely used macromolecular additive that enhances membrane hydrophilicity and pore formation. Its influence is strongly dependent on both concentration and molecular weight. At low concentrations, PVP improves pore connectivity and overall porosity. However, at higher concentrations (≥5 wt%), it increases solution viscosity, which can lead to excessive phase separation and reduced permeability [16]. While high molecular weight PVP contributes to a more defined porous structure, excessive amounts may reduce average pore size and total porosity [17,18]. Additionally, it suppresses macrovoid formation and alters the top layer morphology [19].

The concentration of PSF in the casting solution also plays a critical role in membrane performance. Increasing PSF content typically reduces pore dimensions and water permeability, while enhancing selectivity [20,21]. PEG helps mitigate the intrinsic hydrophobicity of PSF, improving membrane hydrophilicity and modifying macrovoid morphology, which contributes to better selectivity [22–24]. Notably, a casting formulation containing 20% w/w PSF, 25% w/w PEG-400, and 4% w/w acetone yielded a membrane with a highly porous microstructure and a 127% increase in water flux compared to PEG-free membranes [25].

The synergistic use of PEG and PVP as co-additives has been extensively studied. Their combined effect significantly enhances membrane porosity, pore interconnectivity, hydraulic permeability, and solute rejection [26–29]. These additives promote the formation of open microstructures during phase inversion, thereby helping to overcome the inherent trade-off between flux and selectivity in unmodified PSF membranes.

Despite these advancements, achieving an optimal balance between permeability and selectivity in PSF hollow fiber membranes remains a key challenge. Current strategies

often involve copolymer blending, nanoparticle incorporation, or post-treatment modifications, which increase fabrication complexity and cost. Therefore, developing a simple and scalable dope formulation that delivers high-performance asymmetric PSF hollow fibers without additional modification is of practical significance.

In this study, PSF hollow fiber membranes were fabricated via the dry–wet phase inversion method using PEG-400 and high-molecular-weight PVP (Mw ≈ 1,300 kDa) as co-additives. The effects of these additives on membrane morphology, porosity, and filtration performance were systematically investigated. The objective was to establish a minimalist additive strategy capable of achieving high permeability and effective macromolecular rejection, offering a promising approach for industrial-scale ultrafiltration applications.

Materials and Methods

Materials

Polysulfone (PSF, Mw ≈ 35,000 Da) was supplied by BASF SE (Ludwigshafen, Germany) and used as the base polymer. N,N-Dimethylacetamide (DMAc; ≥99.5%, analytical grade, Sigma-Aldrich (St. Louis, Missouri,USA) served as the solvent. Polyethylene glycol (PEG-400; Mw ≈ 400 Da) and polyvinylpyrrolidone (PVP-K90; Mw ≈ 1,300,000 Da) were employed as pore-forming additives. Bovine serum albumin (BSA, Mw ≈ 66 kDa) was obtained from Sigma-Aldrich and used as a model solute for rejection experiments. All chemicals were used as received without further purification, and deionized (DI) water was used through.

Preparation of Dope Solution

The polymer dope solution was prepared by dissolving 25 wt% of PSF in DMAc under continuous stirring at 60 °C for 12 h until complete dissolution was achieved. PEG-400 (22 wt%) and PVP-K90 (0.3 wt%) were then added sequentially to the homogeneous solution while stirring continued to ensure uniform distribution. The final composition of the dope solution was therefore PSF (25 wt%), PEG-400 (22 wt%), PVP (0.3 wt%), and DMAc (52.7 wt%). The mixture was degassed under vacuum for 24 h at room temperature to eliminate trapped air bubbles prior to spinning.

Membrane Fabrication

PSF hollow fiber membranes were fabricated using a dry–wet phase inversion technique. The degassed dope solution was extruded through a double-orifice spinneret (0.3/1.7 mm inner/outer diameters) using nitrogen pressure. Deionized water was used as the bore fluid and the external coagulant. The extrusion rate and bore fluid flow rate were adjusted to ensure a uniform wall thickness. The nascent fibers were drawn through an air gap (~10 cm) before immersion in a deionized water coagulation bath maintained at 22 ± 1 °C. After complete phase inversion, the fibers were rinsed thoroughly with fresh DI water to remove residual solvent and additives, then stored in water prior to characterization. Fig. 1 depicts the schematic of the fabrication apparatus, and Table 1 lists the optimized spinning parameters.

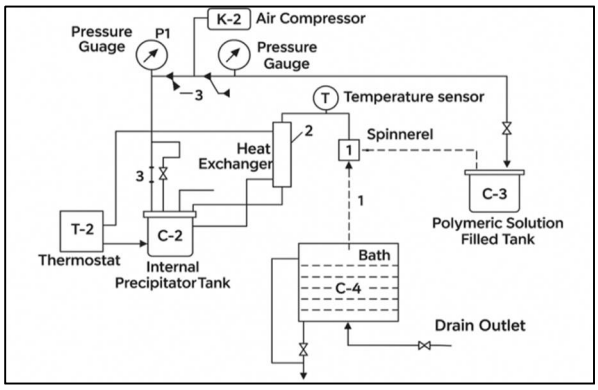

Figure 1. **Schematic diagram of the dry–wet spinning setup used for PSF hollow fiber membrane fabrication, showing the polymer solution delivery, temperature control, and coagulation bath system**

Table 1. **Optimized spinning parameters for the fabrication of PSF hollow fiber membranes, including dope composition, solution properties, and spinning conditions.**

Category	Parameter	Value/ Range	Unit	Remarks
Dope Solution Composition	PSF	25.0	wt.%	Polymer matrix
	PEG-400	22.0	wt.%	Pore-forming additive
	PVP K-90	0.3	wt.%	Pore stabilizer
	DMAc	52.7	wt.%	Solvent
Solution Properties	Viscosity	4800–5200	cP	At room temperature
	Temperature	22 ± 1	°C	During preparation
	Pressure	1.5–2.0	bar	Applied to dope solution
Spinning Conditions	Air gap distance	900	mm	Between spinneret and coagulation bath
	Bore liquid	Water	—	Internal coagulant
	Bore liquid temperature	80	°C	Maintained before spinning
	External coagulant	Water	—	Coagulation medium
	External coagulant temperature	22 ± 1	°C	Room temperature
	Spinneret dimension	0.3 / 1.7	mm	Inner / outer diameter

Membrane Characterization

The morphological and structural characteristics of the fabricated membranes were evaluated using Fourier transform infrared (FT-IR) spectroscopy and scanning electron microscopy (SEM). FT-IR spectra were recorded using a Shimadzu FTIR-8400S spectrophotometer in the range 4000–400 cm^{-1} to confirm chemical stability of the PSF backbone after additive incorporation. SEM imaging (TESCAN MIRA, Czech Republic) was employed to examine surface and cross-sectional morphology.

Samples were fractured in liquid nitrogen, sputter-coated with gold, and observed under an accelerating voltage of 5 kV. The membrane wall thickness was measured from cross-sectional micrographs, while pore structure and morphology were analyzed qualitatively.

Membrane Porosity

The overall porosity (ε, %) of the PSF membrane was determined using the gravimetric ethanol immersion method according to Equation (1):

$$\varepsilon = \frac{V_p}{V_m} \times 100 = \frac{(W_w - W_d)/\rho_{ethanol}}{(W_w - W_d)/\rho_{ethanol} + W_d/\rho_{polymer}} \text{x}100 \quad (1)$$

where W_w and W_d are the wet and dry membrane weights (g), respectively, and $\rho_{ethanol}$ and $\rho_{polymer}$ are the densities of ethanol (0.789 gcm^{-3}) and PSF (1.24 gcm^{-3}). Each measurement was performed in triplicate to ensure reproducibility.

Pure Water Flux Measurement

The pure water flux (PWF) was evaluated using a laboratory-scale cross-flow UF setup, as illustrated schematically in Fig. 2. Distilled water was used as the feed, and measurements were performed at 100 kPa (1 bar) transmembrane pressure under steady-state conditions. The PWF ($Lm^{-2}h^{-1}$) was calculated using Equation (2):

$$J = \frac{V}{A \times t} \quad (2)$$

where V(L) is the permeate volume collected over time t(h), and A(m^2) is the effective membrane area. All flux values were normalized by the applied pressure (bar) to determine the permeability.

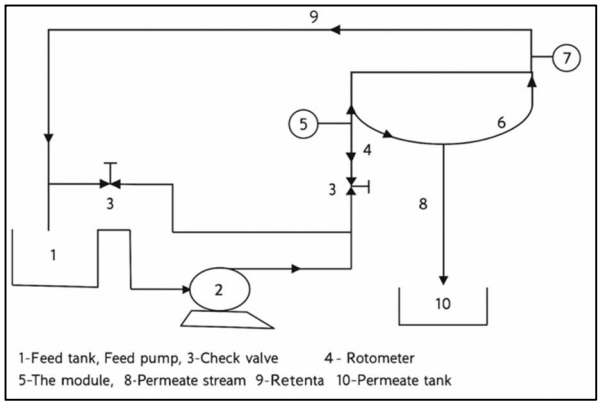

Figure 2. **Schematic diagram of the hollow fiber UF system for PSF membrane testing, showing the feed circulation loop, permeate collection, and retentate recirculation**

BSA Rejection Measurement

The separation capability of the PSF hollow fiber membrane was assessed using a 200 mgL^{-1} BSA aqueous solution (pH 7). The feed solution was circulated through the shell side of the hollow fiber at 1.3 bar, while the permeate was collected from the lumen side at 1 bar. The concentrations of BSA in the feed (C_f) and permeate (C_p) were determined using a Shimadzu UV-2450 spectrophotometer at 280 nm. The rejection rate (R) was calculated using Equation (3):

$$R(\%) = \left(1 - \frac{C_p}{C_f}\right) \times 100 \qquad (3)$$

Each experiment was repeated three times to confirm consistency.

Results and Discussion

The structural integrity, morphological features, and filtration performance of the fabricated PSF hollow fiber membrane were systematically evaluated. FT-IR spectroscopy was employed to verify the preservation of the polymer backbone following additive incorporation, while SEM was utilized to characterize the membrane morphology and elucidate the phase inversion dynamics. Subsequently, filtration efficacy was quantified through measurements of PWF and bovine serum albumin (BSA) rejection.

Structural and morphological characteristic of membrane

FT-IR spectroscopy confirmed the complete preservation of the PSF backbone in the fabricated membrane. As shown in Fig. 3, the broad absorption band observed near 3470 cm^{-1} corresponds to the stretching vibrations of residual –OH groups, which are attributed to physically adsorbed moisture on hydrophilic domains introduced by PEG-400 and PVP during the phase-inversion process. This finding indicates that both pore-forming additives improved the surface affinity toward water without altering the intrinsic PSF chemical structure.

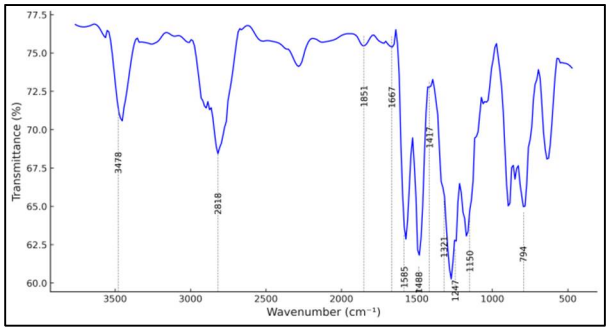

Figure 3. **FT-IR spectrum of the fabricated PSF hollow fiber membrane (4000–400 cm^{-1}) showing characteristic sulfone absorptions at 1320 cm^{-1} (asymmetric O = S = O stretch) and 1150 cm^{-1} (symmetric O = S = O stretch), confirming retention of the polysulfone backbone and absence of new functional groups**

The characteristic fingerprint peaks of PSF were clearly retained in the modified membrane. The distinct absorption bands appearing at approximately 1320 cm^{-1} (asymmetric O═S═O stretching) and 1150 cm^{-1} (symmetric O═S═O stretching) are typical of the sulfone linkage within the PSF matrix, confirming that the sulfone groups remained intact and that no chain scission or oxidative degradation occurred during dope preparation or coagulation [30, 31]. The band detected near 1240 cm^{-1}, assigned to C–O–C

stretching of the aryl–ether bond, together with the aromatic skeletal vibrations observed between 1585–1480 cm^{-1} (C═C stretching), further verifies the chemical integrity of the aromatic PSF backbone [30, 32]. Additionally, the absorption bands within 830–690 cm^{-1}, corresponding to aromatic C–H bending, are consistent with spectra of pristine PSF membranes.

Importantly, no additional peaks or significant wavenumber shifts were observed in the spectra of membranes containing PEG-400 and high-molecular-weight PVP. This confirms that both additives acted purely as physical pore formers, facilitating phase separation and pore development without inducing any chemical modification or covalent interaction with the PSF chains. The preserved spectral pattern demonstrates excellent chemical stability of the polymer matrix, establishing a reliable baseline for its further application in ultrafiltration and separation processes.

SEM analysis revealed a well-defined asymmetric morphology in the hollow fiber membrane. The cross-sectional view (Fig. 4a) depicts an inner lumen with a dense selective skin layer overlying a sponge-like support matrix interspersed with elongated finger-like macrovoids extending across the wall thickness. This structure arises from instantaneous liquid-liquid demixing during phase inversion, where the elevated PSF concentration (25 wt%) enhanced chain entanglement and dope viscosity, thereby accelerating phase separation, facilitating rapid skin formation, and limiting macrovoid proliferation. The finger-like channels provide low-resistance pathways for convective transport, while the sponge-like matrix contributes to mechanical integrity. The overall wall thickness of the hollow fiber was 0.19–0.21 mm, as measured from cross-sectional SEM images obtained at an accelerating voltage of 5 kV, indicating uniform structural integrity typical of wet-spun PSF fibers.

This architecture results from the synergistic effects of PEG-400 (22 wt %), which induces thermodynamic instability and promotes pore interconnectivity, and high-molecular-weight PVP (300 kDa), which moderates solvent–nonsolvent exchange rates. Comparable asymmetric morphologies with dense skins and finger-like voids have been reported for wet-spun PSF fibers, where additive composition and viscosity play critical roles in controlling void propagation and skin thickness [33].

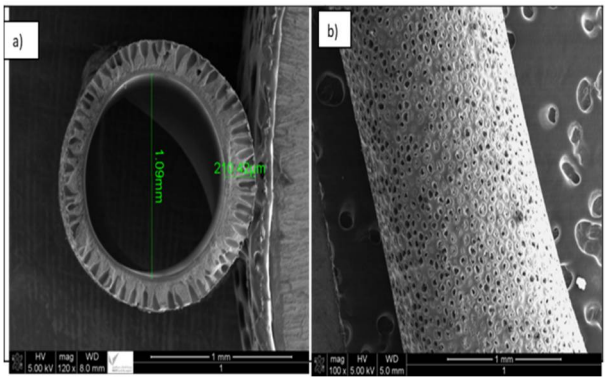

Figure 4. **SEM micrographs of the PSF hollow fiber membrane: (a) cross-sectional view displaying the asymmetric structure with a dense selective skin (~0.5–1 µm) and elongated finger-like macrovoids across the wall; (b) outer surface showing uniform pore distribution that facilitates solvent–nonsolvent exchange and mass transfer**

The outer surface (Fig. 4b) exhibited a uniformly porous texture, indicating efficient solvent–nonsolvent exchange and balanced solidification kinetics. The uniform pore distribution facilitates mass transfer and lowers surface resistance, thereby enhancing permeate flux. Comparable morphologies have been observed where additive ratios dictate top-layer thickness and porosity [34]. The well-controlled asymmetric morphology of the prepared membrane supports the formation of a defect-free selective layer essential for ultrafiltration separations.

Filtration Properties

The fabricated PSF hollow fiber membrane exhibited a porosity of 48.8 ± 2.1%, determined gravimetrically via ethanol immersion, indicating a well-developed porous architecture. The membrane achieved a pure water permeability of 140 $Lm^{-2}h^{-1}$ under a transmembrane pressure of 2 bar, corresponding to a normalized flux of 70 $Lm^{-2}h^{-1}bar^{-1}$. Under steady-state cross-flow conditions at neutral pH, a BSA rejection of 95 ± 1% was recorded, confirming the membrane's classification within the tight ultrafiltration regime. This performance is suitable for macromolecular separations, including protein fractionation and wastewater pretreatment.

The high rejection efficiency is attributed to steric hindrance imposed by the dense top layer, coupled with mild electrostatic (Donnan) interactions between the negatively charged sulfone groups in the PSF matrix and the BSA molecules [3,6,26]. Additionally, the presence of finger-like macrovoids in the substructure facilitates convective transport and reduces internal concentration polarization, thereby sustaining stable flux during operation. This morphological configuration effectively reconciles the inherent trade-off between permeability and selectivity, which typically limits the performance of PSF-based membranes.

As summarized in Table 2, the present hollow-fiber membrane displays superior performance relative to many reported PSF-based systems. Within hollow-fiber configurations, it surpasses the Pluronic F127-modified PSF membrane by Zhou et al. [35], which achieved 83.2 $Lm^{-2}h^{-1}$ and 97.9 % rejection (normalized ≈ 83 $Lm^{-2}h^{-1}bar^{-1}$). Compared with flat-sheet designs, the current membrane demonstrates an optimized flux–rejection balance. Conventional unmodified PSF flat-sheets exhibit normalized fluxes around 29 $Lm^{-2}h^{-1}bar^{-1}$ with ≈97 % BSA rejection [36], while PSF/HA blends reach 45.5–63 $Lm^{-2}h^{-1}bar^{-1}$ at 97.2 % rejection [37]. Although zwitterionic PSF [38] and TCPP-modified PSF flat-sheets [39] report much higher fluxes (420–614 $Lm^{-2}h^{-1}$), their complex surface modifications raise cost and scalability concerns. In contrast, the dual-additive formulation used here achieves comparable BSA rejection (≈95–98 %) with simple processing.

Table 2. **Comparative filtration performance of PSF-based ultrafiltration membranes, highlighting the superior permeability (140 $Lm^{-2}h^{-1}$) and balanced rejection (95%) of the present hollow fiber membrane relative to reported PSF and modified flat-sheet systems *(N/S : not specified)* .**

Membrane Type	Porosity (%)	Wall Thickness (mm)	PWP (LMH)	TMP (bar)	Normalized Flux (LMH/bar)	BSA Rejection (%)	Reference
PSF HF	48.8	0.19–0.21	140	2	70	95	This work
Modified PSF HF	N/S	N/S	83.2	~1	~83	97.9	[35]
PSF flat-sheet	N/S	N/S	~70	2.4	~29	~97	[36]
PSF/HA blend flat-sheet	N/S	N/S	N/S	2	45.5–63	97.2	[37]
Zwitterionic PSF flat-sheet	N/S	N/S	N/S	N/A	420.4	>95	[38]
TCPP-modified PSF flat-sheet	N/s	N/S	N/S	1	614	>95	[39]
PES/FS blend flat-sheet	N/S	N/S	61.2	2	30.6	95	[40]
ZSM-5 PSF flat-sheet	N/S	N/S	394.7	3	131.6	>98	[41]
Zwitterionic PSE HF	N/S	N/S	140	~2	~70	>97	[42]

When compared to PES/FS blends [40] and ZSM-5-incorporated PSF membranes [41], the developed membrane exhibits higher normalized flux (70 vs 30–132 $Lm^{-2}h^{-1}bar^{-1}$) while maintaining consistent rejection, indicating that the PEG-400/PVP combination effectively enhances hydrophilicity and pore connectivity. The membrane also performs comparably to the zwitterionic PSE hollow-fiber system [42], despite the latter relying on copolymer blending, highlighting the robustness and scalability of this minimalist dual-additive approach.

The optimized morphology arises from synergistic interactions between PEG-400 and high-molecular-weight PVP. PEG-400 accelerates phase separation and establishes interconnected pore channels, while trace PVP (0.3 wt%, ≈300 kDa) moderates demixing to produce a thin selective skin (≈0.5–1 µm) and suppress excessive macrovoids [43, 44]. This yields a hydrophilic surface (contact angle < 60°) and a well-developed pore network that mitigates the conventional permeability–selectivity trade-off [45]. Residual PVP enhances antifouling, reflected in >85 % flux recovery after BSA filtration [45].

In addition to hydraulic advantages, the membrane demonstrates ≈50% greater packing density and intrinsic self-cleaning under cross-flow conditions [46, 47], further improving process continuity. Collectively, these attributes make the fabricated PSF hollow-fiber membrane a cost-effective and scalable candidate for continuous ultrafiltration in water purification and bioprocessing applications [48].

Conclusion

PSF hollow fiber membranes were successfully fabricated making use of dry–wet phase inversion technique from a dual-additive system of PEG-400 and high-molecular-weight PVP. The obtained membranes exhibited a well-developed asymmetric structure with a thin selective skin (~0.5–1 µm), interconnected finger-like macrovoids, and a total wall thickness of 0.19–0.21 mm. FT-IR spectra confirmed the preservation of the PSF backbone, which indicate that the additives acted as physical pore formers without chemical modification. The optimized membrane demonstrated a porosity of 48.8 ± 2.1%, a pure-water permeability of 140 $Lm^{-2}h^{-1}$ at 2 bar, and a BSA rejection of 95 ± 1%. These results correspond to a tight-ultrafiltration regime, suitable for macromolecular separations such as protein fractionation and water purification. Comparative analysis with existing literature demonstrates that the minimalist dual-additive formulation—comprising PEG-400 and trace PVP—achieves permeability and solute rejection performance on par with more chemically complex PSF membrane systems. This approach offers advantages in fabrication simplicity and cost-efficiency. The synergy between PEG-400 and trace PVP promotes rapid phase separation and improved pore connectivity. This also enhances surface hydrophilicity, resulting in strong antifouling performance with over 85% flux recovery after BSA filtration. Therefore, the developed PSF hollow fiber membrane is structurally robust and delivers high, consistent flux. It has a potential for industrial ultrafiltration in bioprocessing, dairy clarification, and RO/NF pretreatment.

Acknowledgements

The authors thank King Abdulaziz City for Science and Technology (KACST) for funding this study (Project No. 29-253).

Conflict of Interest

The authors declare no conflict of interest.

References

1. J. M. Laine, D. Vial and P. Moulart, *Desalination*, 131 (2000) 17. https://doi.org/10.1016/S0011-9164(00)90002-X
2. B. Kwon, J. Cho, N. Park and J. Pellegrino, *J. Membr. Sci.,* 279 (2006) 209. https://doi.org/10.1016/j.memsci.2005.12.007.
3. Z. L. Xu and F. A. Qusay, *J. Membr. Sci.,* 233 (2004) 101. https://doi.org/10.1016/j.memsci.2004.01.005
4. J. J. Qin, F. S. Wong, Y. Li and Y. T. Liu, *J. Membr. Sci.,* 211 (2003) 139. https://doi.org/10.1016/S0376-7388(02)00415-5
5. Y. Liu, G.H. Koops and H. Strathmann, *J. Membr. Sci.,* 223 (2003) 187. https://doi.org/10.1016/S0376-7388(03)00322-3
6. Q. Z. Zheng, P. Wang and Y. N. Yang, *J. Membr. Sci.,* 279 (2006) 230. https://doi.org/10.1016/j.memsci.2005.12.009
7. E. Saljoughi, M. Amirilargani and T. Mohammadi, *Desalination,* 262 (2010) 72. https://doi.org/10.1016/j.desal.2010.05.046
8. J. H. Kim and K. H. Lee, *J. Membr Sci.,* 138 (1998) 153. https://doi.org/10.1016/S0376-7388(97)00224-X
9. M. Amirilargani, E.Saljoughi, T. Mohammadi, *Desalination,* 249 (2009) 837. https://doi.org/10.1016/j.desal.2009.01.041
10. M. Rahbari-Sisakht, A. F. Ismail and T. Matsuura, *Sep. Purif. Technol.,* 88 (2012) 99. https://doi.org/10.1016/j.seppur.2011.12.012
11. V. Laninovich, *Desalination,* 186 (2005) 39. https://doi.org/10.1016/j.desal.2005.01.017
12. J. J. Shieh, T. S. Chung, R. Wang, M. P. Srinivasan and D. R. Paul, *J. Membr. Sci.,* 182 (2001) 111. https://doi.org/10.1016/S0376-7388(00)00560-3
13. M. Yuxin, S. Fergnei, M. Jun, W. Miaonan, Z. Jun and G. Congjie, *Desalination,* 51 (2011) 272. https://doi.org/10.1016/j.desal.2010.12.054
14. B. Chakrabarty, A. K. Ghoshal and M. K. Purkait, *J. Membr. Sci.,* 209 (2008) 309. https://doi.org/10.1016/j.memsci.2007.10.027
15. I. Cabasso, E. Klein and J. K. Smith, *J. Appl. Polym. Sci.,* 20 (1976) 2377. https://doi.org/10.1002/app.1976.070200908
16. N. N. Aminudin, H. Basri, Z. Harun and M. Z. Yunos, *J. Teknol.,* 65 (2013) 47. https://doi.org/10.11113/jt.v65.2327
17. M. J. Han and S. T. Nam, *J. Membr. Sci.,* 202 (2002) 55. https://doi.org/10.1016/S0376-7388(01)00718-9
18. B. Chakrabarty, A. K. Ghoshal and M. K. Purkait, *J. Membr. Sci.,* 315 (2008) 36. https://doi.org/10.1016/j.memsci.2008.02.027.
19. D. B. Mosqueda-Jimenez, R. M. Narbaitz, T. Matsuura, G. Chowdhury, G. Pleizier and J. P. Santerre, *J. Membr. Sci.,* 231 (2004) 209.

https://doi.org/10.1016/j.memsci.2003.11.026
20. B. Jung, J. K. Yoon, B. Kim and H. W. Rhee, *J. Membr. Sci.,* 243 (2004) 45. https://doi.org/10.1016/j.memsci.2004.06.011.
21. H. L. Huang and S. Yang, *J. Aerosol Sci.,* 37 (2006) 1198. https://doi.org/10.1016/j.jaerosci.2005.11.004 Incorrect DOI
22. Y. Xu, B. Zhu and Y. Xu, *Polymer,* 46 (2005) 713. https://doi.org/10.1016/j.polymer.2004.12.001
23. I. Ahmed, A. Idris and N. F. Che Pa, *J. Appl. Polym. Sci.,* 115 (2010) 1428. https://doi.org/10.1002/app.31061.
24. P. J. Brown, S. Ying and J. Yang, *Autex Res. J.,* 2 (2002) 101. https://doi.org/10.1515/aut-2002-020206.
25. D. Wang, K. Li and W. K. Teo, *J. Membr. Sci.,* 147 (2000) 176. https://doi.org/10.1016/S0376-7388(00)00438-0
26. A. Urkiaga, D. Iturbe and J. Etxebarria, *Desalination Water Treat.,* 56 (2015) 3415. https://doi.org/10.1080/19443994.2014.1000976
27. K. A. Gebru and C. Das, *Chin. J. Chem. Eng.,* 25 (2017) 911. https://doi.org/10.1016/j.cjche.2016.11.017
28. D. Shanthana Lakshmi, R. K. S. Radha, R. Castro-Muñoz and M. Tańczyk, *Polymers,* 14 (2022) 5209. https://doi.org/10.3390/polym14235209
29. N. Nasrollahi, L. Ghalamchi, V. Vatanpour, A. Khataee and M. Yousefpoor, *J. Ind. Eng. Chem.,* 109 (2022) 100. https://doi.org/10.1016/j.jiec.2022.02.036
30. M. K. Paidi, V. Polisetti, K. Damarla, P. S. Singh, S. K. Mandal and P. Ray, *Polymers*, 14 (2022) 1750. https://doi.org/10.3390/polym14091750.
31. Y. Jiang, Q. Zeng, P. Biswas and J. D. Fortner, J. Membr. Sci., 581 (2019) 453 https://doi.org/10.1016/j.memsci.2019.03.056
32. T. Rasmussen, *Membranes,* 13 (2023) 465. https://doi.org/10.3390/membranes13050465.
33. N. Peng, T. –S. Chung, K. Y. Wang, *J. Membr. Sci.,* 318 (2008) 363. https://doi.org/10.1016/j.memsci.2008.02.063
34. T. V. Plisko, A. V. Bildyukevich, L. Zhao, W. Huang, V. V. Volkov, Z. Huang, *Fibers* 9 (2021) 28. https://doi.org/10.3390/fib9050028.
35. C. H. Loh, R. Wang, L. Shi and A. G. Fane, *J. Membr. Sci.,* 380 (2011) 114. https://doi.org/10.1016/j.memsci.2011.06.041.
36. C. Hackett, D. Hale, B. Bair, G.-D. Manson-Endeboh, X. Hao, X. Qian and S. R. Wickramasinghe, *Sep. Purif. Technol.,* 332 (2024) 125752. https://doi.org/10.1016/j.seppur.2023.125752
37. A. J. Clarke, A. Dickson, D. P. Dowling, *Polymers,* 16 (2024) 63. https://doi.org/10.3390/polym16010063
38. J. Wang, Z. Wang, Y. Liu, J. Wang and S. Wang, *J. Membr. Sci.,* 514 (2016) 407. https://doi.org/10.1016/j.memsci.2016.05.014
39. J. A. Prince, S. Bhuvana, V. Anbharasi, N. Ayyanar, K. Boodhoo and G. Singh, *Sci. Rep.,* 4 (2014) 6555. https://doi.org/10.1038/srep06555.
40. Y-J. Won, D.-C. Choi, J. H. Jang, J.-W. Lee, H. R. Chae, I. Kim, K. H. Ahn, C.-H. Lee and I.-C. Kim, *J. Membr. Sci.,* 462 (2014) 1.

https://doi.org/10.1016/j.memsci.2014.03.012.
41. G. P. Syed Ibrahim, A. M. Isloor, A. Al Ahmed and B. Lakshmi, *J. Appl. Membr. Sci. Technol.,* 18 (2016) 25. https://doi.org/10.11113/amst.v18i1.17
42. K. Guan, K. Ushio, K. Nakagawa, T. Shintani, T. Yoshioka, A. Matsuoka, E. Kamio, W. Jin and H. Matsuyama, *J. Membr. Sci.,* 660 (2022) 120861. https://doi.org/10.1016/j.memsci.2022.120861
43. N. N. Aminudin, H. Basri, Z. Harun and M. Z. Yunos, *J. Teknologi: Sci. Eng.,* 65 (2013) 47. doi: 10.11113/jt.v65.2327.
44. T. V. Plisko, A. V. Bildyukevich, L. Zhao W. Huang, V. V. Volkov, Z.Huang, *Membr.,* 9 (2021) 28. https://doi.org/10.3390/membranes9050028
45. D. Yu, Y. Liang, T. N. Rathmalgodagei, T. Ritigala and Y. Wei, *Membranes,* 11 (2021) 100. https://doi.org/10.3390/membranes11020100
46. M. K. Hosseini, L. Liu, A. Bhattacharyya, K. Lee, J. Miao and B. Chen, *J. Mar. Sci. Eng.,* 10 (2022) 1313. https://doi.org/10.3390/jmse10091313
47. A. A. A. Ismail, S. Mulyati, S. Aprilia, M. H. M. Yusoff, N. I. M. Nawi, M. R. Bilad, A. F. Isamil, N. Arahman, *Water,* 12 (2020) 3533. https://doi.org/10.3390/w12123533.
48. J. A. Prince, S. Bhuvana, V. Anbharasi, N. Ayyanar, K. Boodhoo and G. Singh, *Sci. Rep.,* 4 (2014) 6555. https://doi.org/10.1038/srep06555